ISSN 2321-807X
Volume 12 Number14
Journal of Advances in chemistry

Synthesis, Characterization and Inhibitive Effect of 1-[(4-methylPhenyl) Sulfonyl]-4-pyridine-2-ylpiperazine on Corrosion of Mild Steel in HCl Medium

P. Sumathi[1 *], K. Kannan[2], S. Gnanavel[2], S. Anbuselvi[3]
[1] Department of Chemistry, Knowledge Institute of Technology, Salem, Tamilnadu, India
[*]E-mail: sumathi.murugan25@gmail.com
[2] Department of Chemistry, Government College of Engineering, Salem, Tamilnadu, India
E-mail: kannan_k2002@yahoo.co.in
E-mail: gnanamphd@gmail.com
[3] Department of Chemistry, Sri Sarada College for Women, Salem, Tamilnadu, India
E-mail: selvisarachem80@gmail.com

ABSTRACT

A novel inhibitor, 1-[(4-methylphenyl)Sulfonyl]-4–pyridine-2-ylpiperazine (MSPP) has been synthesized and characterized using FT-IR, ^{1}H NMR,^{13}C NMR , LC-MS and UV-visible spectroscopy methods.The inhibitive effect of 1-[(4-methylphenyl)sulfonyl]-4-pyridin-2-ylpiperazine(MSPP) on the corrosion of mild steel in 1M HCl was investigated by weight loss, potentiodynamic polarization and electrochemical impedance spectroscopy (EIS) techniques. The efficiency of the inhibitor increases with the increase in the inhibitor concentration and decrease with a rise in temperature. Potentiodynamic polarization study showed that the inhibitor acts as mixed type. EIS finding showed that the change in the impedance parameters (R_{ct} and C_{dl}), with the variation in MSPP concentration is due to the adsorption of active molecules leading to the formation of protective layer on the surface of mild steel. The UV-visible absorption spectra indicate the formation of a MSPP-Fe complex. The adsorption data fitted with Langmuir adsorption isotherm. Thermodynamic parameters such as activation energy (E_a), free energy change (ΔG_{ads}), enthalpy change (ΔH_{ads}) and entropy change (ΔS_{ads}) were also evaluated and discussed in detail. Surface analysis by AFM and SEM confirmed the formation of protective coating on the mild steel surface. Quantum chemical calculation were also performed using density functional theory.

Keywords HCl, Mild steel, corrosion, inhibition, EIS, DFT

1. INTRODUCTION

Corrosion is a common problem for mild steel in our life time application and directly impacts its cost and safety [1]. Corrosion inhibition of mild steel is a matter of theoretical as well as practical importance. Mild steel is widely used in industries because of its low cost and easy availability in ease for the fabrication of various reaction vessels such as cooling tower tanks, pipelines, and other important fields of application are acid pickling, industrial cleaning, acid descaling, oil recovery and petrochemical process, large tonnages in marine application, chemical processing, construction and metal processing equipment [2-6]. Various methods are used to decrease the corrosion rate of metals in acids, among those methods use of inhibitors is common, involving in the formation of passivation layer which prevent the corrosion.[7-8] Organic compounds that contain sulphur, nitrogen and oxygen atoms are able to retard metallic corrosion.

The compound which have π bonds and compound containing N, S and O have been reported as effective and efficient corrosion inhibitor [9-15].

The strength of adsorbed layer is related to the functional groups connected to aromatic ring [16]. The adsorption of organic compounds depends mainly on the electronic structure of the molecule and that the inhibition efficiency increases with the increase in the number of aromatic ring [17]. The most favorable qualities possessed by compounds to act as efficient inhibitors are they should be adsorbed on metallic surface in acid solution, should slow down the cathodic reaction as well as the anodic process of dissolution of the metal and should form a compact barrier films on the surface, block the active sites and thereby reduce the corrosion rate of the metal by adsorption. They should have high adsorption energy [18-19]. which depends on the strength and the nature of the bonds formed between the inhibitor molecules and the metal surface. Molecules that contain both nitrogen and sulphur are of particular importance since these provide an excellent inhibition in comparison with the compound containing either sulphur or nitrogen [(20)] In case of corrosion in an acid medium, the corrosion rate increases with temperature because the hydrogen evolution over potential decreases [21].

The present study aims to investigate the inhibiting effect of MSPP on corrosion of mild steel in 1 M HCl solution. This compound has three nitrogen, two oxygen and one sulphur group which are very essential for an organic compound to behave as an effective corrosion inhibitor .The inhibition efficiency of this compound was studied by weight-loss, Potentiodynamic polarization and electrochemical impedance spectroscopy. The thermodynamic functions for the dissolution and adsorption were investigated and further confirmation of inhibitive action was done by scanning electron microscopy and atomic fore microscopy (AFM) analysis. The relationship between the inhibition efficiency of MSPP in the investigated acidic solution and some quantum chemical parameters (such as HOMO, LUMO energies and dipole moment) have also been studied.

2. EXPERIMENTAL

2.1. Synthesis 1-[(4-methylphenyl)sulfonyl]-4-pyridin-2-ylpiperazine

To the dichloroethane solvent (60ml) 1-(Pyridin-2-yl)piperazine (3 g, 0.0184 mol) was added and followed by the solution of p- Toluenesulfonylchloride (4.19g, 0.0220mol) with pyridine(7.26ml, 0.092mol) at 0^{o}C under nitrogen atmosphere, The resulting reaction mixture was allowed to stirring at room temperature for 2hrs, then the reaction was extracted by ethyl acetate and washed by dil H_2O and then by brine solution. Then the again organic layer was dried by anhydrous Na_2SO_4 and the solvent was removed under reduced pressure afforded a yellow product 37 % yield (1.2g) FT-IR ,^{1}H and ^{13}C NMR and mass spectra has been recorded and confirmed the structure of the compound. Figure 1 represents the synthesis of MSPP.

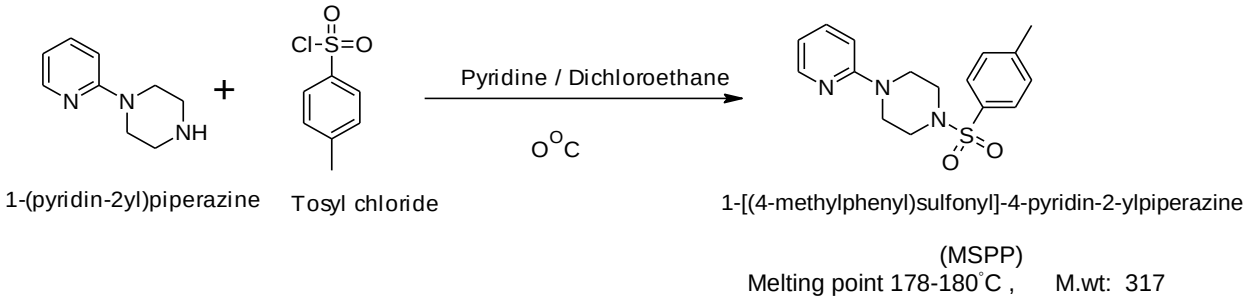

Figure 1. Synthesis of MSPP

2.2 Structural Elucidation (FT-IR, NMR and TGA)

The FT-IR spectra were recorded on a Spectrum RXI Make Perkin Elmer FT-IR spectrophotometer in the rang 4000 cm -1 to 400 cm-1 in KBr pellet. The 1H NMR and 13C NMR spectra were recorded on a Bruker AC 300F (300 MHz) NMR spectrometer using DMSO as solvent and TMS as an internal standard. The TGA and DSC Instruments Model SDT Q600 provided information about the thermal stability and thermal decomposition of MSPP.

2.3 Weight loss studies

A clean weighed mild steel specimen was completely immersed in the solution by hanging from the glass rod using Teflon thread for different time intervals (1 h, 2 h, 3 h and 4 h) without and with inhibitor at 303K. The same procedure was repeated for different temperatures (303 K, 313 K, 323 K and 333K)with immersion period of 1 h.

2.3.1 Corrosion Rate

$$CR = \frac{8.76X10{,}000W}{ATD} \qquad (1)$$

Where W= weight loss of test specimen in g; A= area of test specimen in cm2, T= time of exposure in hrs; D=density of material in gcm−3, CR=corrosion rate in mmpy.

2.4 potentiodynamic polarization

The electrochemical behaviour of mild steel in inhibited and uninhibited solutions was studied by recording anodic and cathodic potentiodynamic polarization curves using. The exposed area was washed with distilled water, degreased with trichloroethylene and finally washed with water. Polarization measurements were obtained at a scan rate of 0.2 mV/ s using electrochemical analyzer Model CHI608D\E instrument.

2.5 Electrochemical Impedance spectroscopy

The electrochemical measurements were carried out in a three electrode cell assembly. Platinum and saturated calomel electrodes were used as counter and reference electrodes respectively. The same mild steel specimen in the form of cylindrical rod, embedded in Teflon, with an exposed area of 1cm^2 was used as working electrode. The Rct (charge transfer resistance) and Cdl (double layer capacitance) values were calculated. Cdl (double layer capacitance) values were calculated using the relationship (2).

$$Cdl = \frac{1}{2X3.14Xf\ \max\ XRct} \qquad (2)$$

2.6 UV visible Spectroscopy studies

UV-Visible absorption spectral measurements were carried out on the prepared mild steel samples after immersion in 1M HCl without and with inhibitor of MSPP at 303 K for 4 hr using a (mode: Lambda 35) Perkin-Elmer UV-Visible spectrophotometer.

2.7 Surface Analysis (SEM, AFM and XRD)

The morphology of treated mild steel surface was examined by using scanning electron microscope(Model:VEGA3 TESCAN), atomic force microscopy(Model: PicoSPM – Picoscan 2100) and X- ray diffraction analysis (Model: PW3040/60 X'pert PRO).

2.8 Quantum chemical parameters

The Quantum chemical parameters for the PTC obtained using DFT at the B3LYP/6-311G (d,p) basis set and semi empirical (PM6) method by standard Gaussian 03 software package such as the energy of the highest occupied molecular orbital (HOMO), the energy of the lowest unoccupied molecular orbital (LUMO), ΔEgap and dipole moment (μ), absolute electronegativity (χ) and electrophilicity (ω) were calculated.

3. RESULTS AND DISCUSSION

3.1. Characterization of MSPP

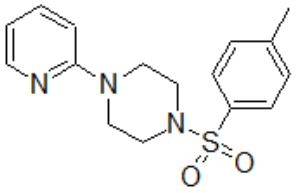

Figure 2. Structure of MSPP

Yield 92% yellow solid., ^{1}H NMR (400 MHz, DMSO-d6) d(ppm): 2.38 (3H, CH_3), 2.91-2.94 (4H, t, piperazine CH_2), 3.56-3.58 (4H, t, piperazine CH_2), 6.41-6.44 (1H, m, pyridne), 6.78-6.80 (1H, d, pyridine), 7.42-7.44 (1H, d, phenyl), 7.48-7.52 (1H, m, pyridine), 7.61-7.64 (2H, d, phenyl), 8.05-8.06 (1H, m, pyridine); ^{13}C NMR (100 MHz, DMSO-d6) d(ppm): 20.9, 44.0, 45.5, 107.5, 113.5, 127.6, 129.8, 131.8, 137.7, 143.7, 147.3, 158.2; MS (EI): m/z calc for C16H19N3O2S: 317.12; Found: 318.02. IR (KBr, vmax cm^{-1}): 3431, 2989, 1594, 1480, 1438; Figure 3(a-b) show the ^{1}H NMR(3a), ^{13}C NMR(3b), Mass spectrum (3c) and FT-IR spectra(3d) spectra of MSPP. The spectral data are shown above. From the data the structure of MSPP is confirmed.

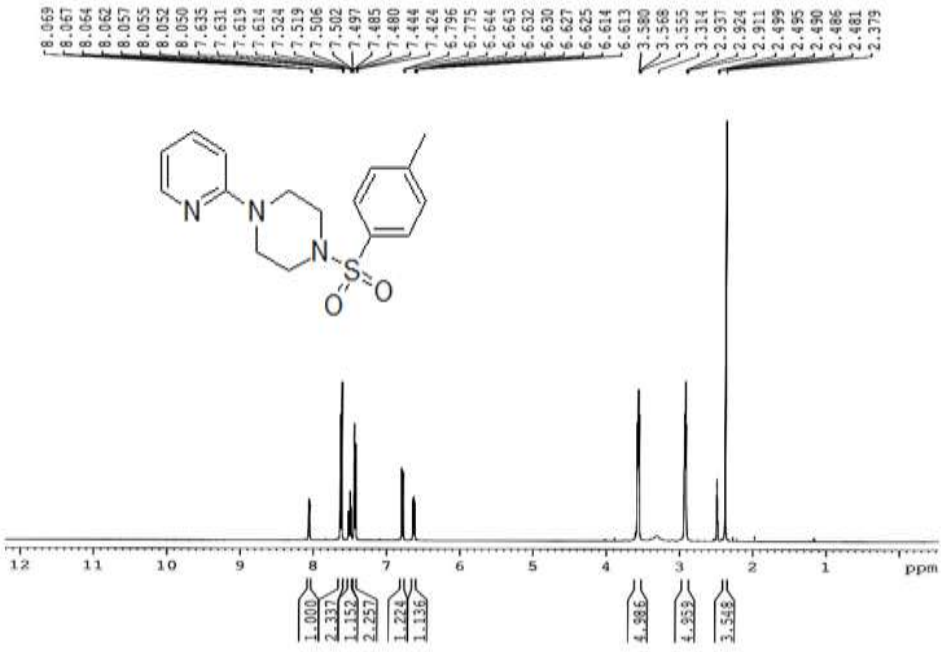

Figure 3a. ^{1}H NMR spectrum of MSPP.

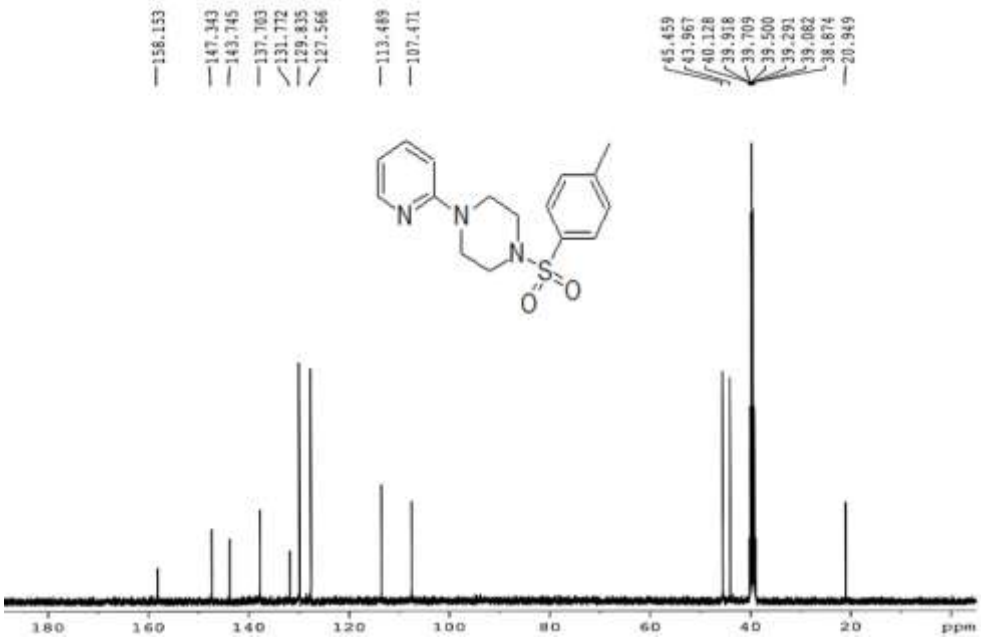

Figure 3b. ^{13}C NMR spectrum of MSPP.

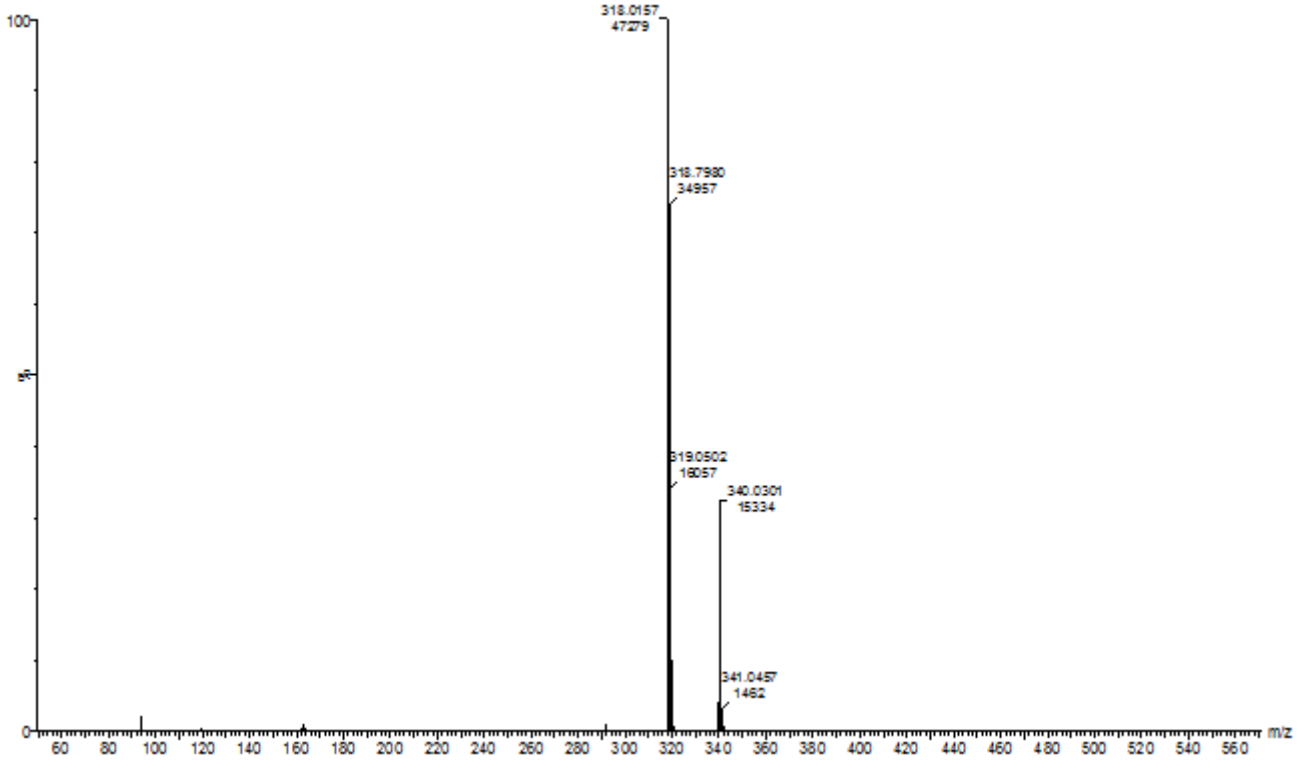

Figure 3c. Mass spectrum of MSPP.

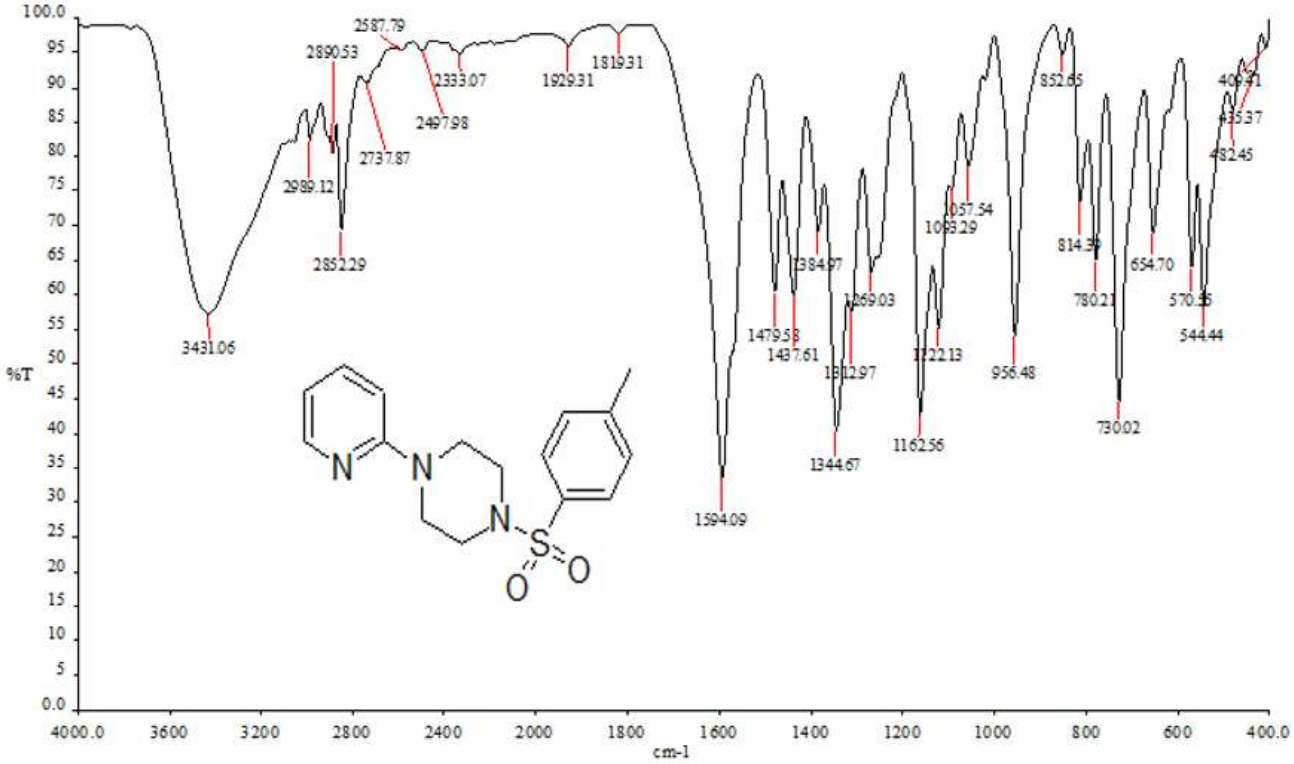

Figure 3d. FT-IR spectrum of MSPP

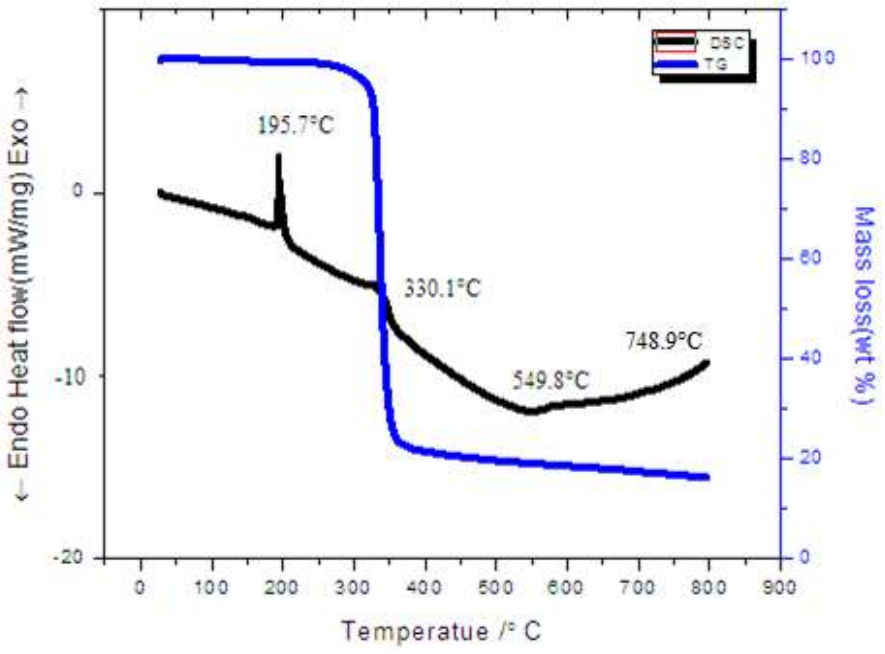

Figure 4. TGA and DSC curves of MSPP

From the TG-DSC analysis of a compound exhibiting a simple melt, data from MSPP is presented in Figure 3.21 shows an overlay of the DSC and TGA data in which the TGA curve show that the thermal decomposition of MSPP occurs in the temperature 358.7°C with the TG % of ~ 24.4%. In the DSC curve, endothermic peaks occur at 549.8°C corresponding to fusion and decomposition processes of the compound MSPP. This peak is caused by the decomposition of the compound MSPP. The presence of an endothermic peak shows the desorption of water molecules from the MSPP. The exothermic peak at 195.7 °C corresponds to the crystallisation of MSPP.

3.2. Corrosion studies

3.2.1. Weight loss studies

Weight loss in mg/cm^2 of the surface area for mild steel in 1M HCl solution was determined in the absence and presence of the inhibitor MSPP.

Surface Coverage (θ) = W_0 -W /W_0 (3)

Inhibition Efficiency (IE %) = (W_0 -W /W_0) X 100 (4)

W_0 and W are weight loss values in the absence and presence of the inhibitor. The weight loss measurements were also carried out at different time intervals, different concentrations of the acid solutions and at different temperatures.

Table 1. Weight loss measurement parameters for mild steel in 1M HCl in the absence and presence of MSPP at 1-4h (303K)

Conc of MSPP (ppm)	Corrosion rate (mmpy)				Surface coverage(Θ)				Inhibition efficiency (%)			
	1hr	2hr	3hr	4hr	1hr	2hr	3hr	4hr	1hr	2hr	3hr	4hr
Blank	62.343	78.189	140.755	241.932	-	-	-	-	-	-	-	-
100	6.026	5.282	4.985	4.761	0.9033	0.9324	0.9646	0.9803	90.33	93.24	96.46	98.03
200	5.059	4.538	4.315	4.464	0.9189	0.9420	0.9693	0.9815	91.89	94.20	96.93	98.15
300	4.166	3.794	3.645	3.720	0.9332	0.9515	0.9741	0.9846	93.32	95.15	97.41	98.46
400	3.199	2.901	2.753	2.753	0.9487	0.9629	0.9804	0.9886	94.87	96.29	98.04	98.86
500	2.678	2.381	2.232	2.158	0.9570	0.9696	0.9841	0.9911	95.70	96.96	98.41	99.11
600	2.158	1.934	1.860	1.637	0.9654	0.9753	0.9868	0.9932	96.54	97.53	98.68	99.32
700	2.083	1.860	1.637	1.339	0.9666	0.9762	0.9884	0.9945	96.66	97.62	98.84	99.45
800	1.860	1.488	1.339	1.265	0.9702	0.9810	0.9905	0.9948	97.02	98.10	99.05	99.48
900	1.116	0.893	0.744	0.595	0.9821	0.9886	0.9947	0.9975	98.21	98.86	99.47	99.75

The values of weight loss, inhibition efficiency (IE%) and the corrosion rate (CR) obtained from weight loss method at different concentrations (100-900 ppm) of MSPP for various immersion periods of 1h, 2h, 3h and 4h at constant temperature (303K) are summarized in table-1 and Fig 5 . It is noticed from the table that the weight loss decreased with increasing inhibitor concentration due to the blocking effect of the surface by both adsorption and film formation mechanisms, which decreases the effective area of corrosion attack [22]. It is also observed that corrosion rate decreased with increase in inhibitor concentration and increased with increasing temperatures. The maximum inhibition efficiency of (MSPP) inhibitor was found to be 99.75 % for 900 ppm on optimum inhibitor concentration at 4h.

Table 2. Calculated values of corrosion rate, surface coverage and inhibition efficiency for mild steel in 1M HCl in the presence and absence of MPSS at 303-333K (1hour)

Conc of MSPP (ppm)	Corrosion rate (mmpy)				Surface coverage(Θ)				Inhibition efficiency (%)			
	303 (K)	313(K)	323(K)	333(K)	303(K)	313(K)	323(K)	333(K)	303(K)	313(K)	323(K)	333(K)
Blank	62.343	196.775	317.666	552.308	-	-	-	-	-	-	-	-
100	6.026	70.452	147.748	295.348	0.9033	0.642	0.5349	0.4652	90.33	64.2	53.49	46.52
200	5.059	45.381	119.85	226.607	0.9189	0.7694	0.6227	0.5897	91.89	76.94	62.27	58.97
300	4.166	29.684	66.212	146.409	0.9332	0.8491	0.7916	0.7349	93.32	84.91	79.16	73.49

400	3.199	29.386	46.571	132.646	0.9487	0.8534	0.8507	0.7598	94.87	85.34	85.07	75.98
500	2.678	22.17	35.71	96.639	0.957	0.8873	0.8876	0.825	95.7	88.76	88.73	82.5
600	2.158	16.962	34.445	78.635	0.9654	0.9138	0.8916	0.8576	96.54	91.38	89.16	85.76
700	2.083	9.002	23.583	74.916	0.9667	0.9543	0.9258	0.8644	96.67	95.43	92.58	86.44
800	1.86	6.547	16.962	70.08	0.9702	0.9566	0.9466	0.8731	97.02	95.66	94.66	87.31
900	1.116	5.505	14.656	59.739	0.9821	0.972	0.9539	0.8918	98.21	97.2	95.39	89.18

From the data it is clearly seen that the corrosion rate of mild steel depends upon two factors namely, inhibitor concentration and temperature. The results are given in table 2. The inhibition efficiency decreases and corrosion rate increases with increasing the solution temperature from 303 to 333K.This can be attributed to increased rate of desorption of inhibitor molecules from the surface of mild steel with increasing temperature. This means that this MSPP has a significant decrease in its protective properties with raising temperature. These results confirmed that (MSPP) acts as a good inhibitor for mild steel in 1M hydrochloric acid solution in the range of temperature studied, which gives optimum inhibition efficiency values as high as 98.21% in room temperature.

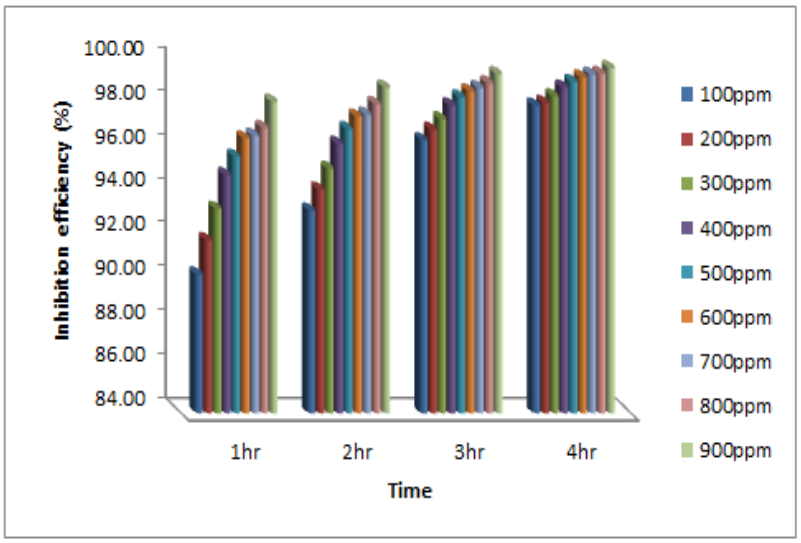

Figure 5. Inhibition efficiency vs Time for mild steel in 1M HCl solution in the presence of different concentrations of MSPP for 1- 4hr (303K).

3.2.2 Potentiodynamic polarization measurements

The potentiodynamic polarization curves for mild steel in 1M HCl solution with different concentrations of inhibitor at 303 K are shown in Fig 6. The values associated with electrochemical parameters and inhibition efficiency (IE%) values were calculated from polarization curves and listed in Table 3 It is clearly by noticed that introduction of MSPP inhibitor into the corrosive medium cause a reduction of both cathodic and anodic current densities (decreases the corrosion rate), i.e., shifts the anodic curves to more positive potentials and the cathodic curves to more negative potentials. The inhibition efficiency was calculated by the following equation (5).The inhibition efficiency value is also found to increase from 89.16 % to 97.36%. The addition of inhibitors reduced anodic dissolution and also retards the hydrogen evolution reaction.

$$IE\% = \frac{I_{(uninh)} - I_{(inhi)}}{I_{(uninh)}} X100 \qquad (5)$$

where $I_{uninh.}$ and $I_{inh.}$ are corrosion current densities in the absence and presence of the inhibitor, respectively. Lower corrosion current densities (I_{corr}) were observed in the presence of studied MSPP compound (0.1049 mA cm^2 at 900 ppm) with respect to the blank solution (3.981 mA cm^2) due to increase in the adsorption of the inhibitor molecule on to the metal surface. Further the E_{corr} value shifts to positive direction but no significant change is observed, which indicate that hydrogen evolution reaction is activation controlled and the addition of the studied MSPP does not modify the mechanism of this process [23]. Addition of the MSPP affects both anodic and cathodic reaction. Therefore, this compound could be classified as a mixed type inhibitor.

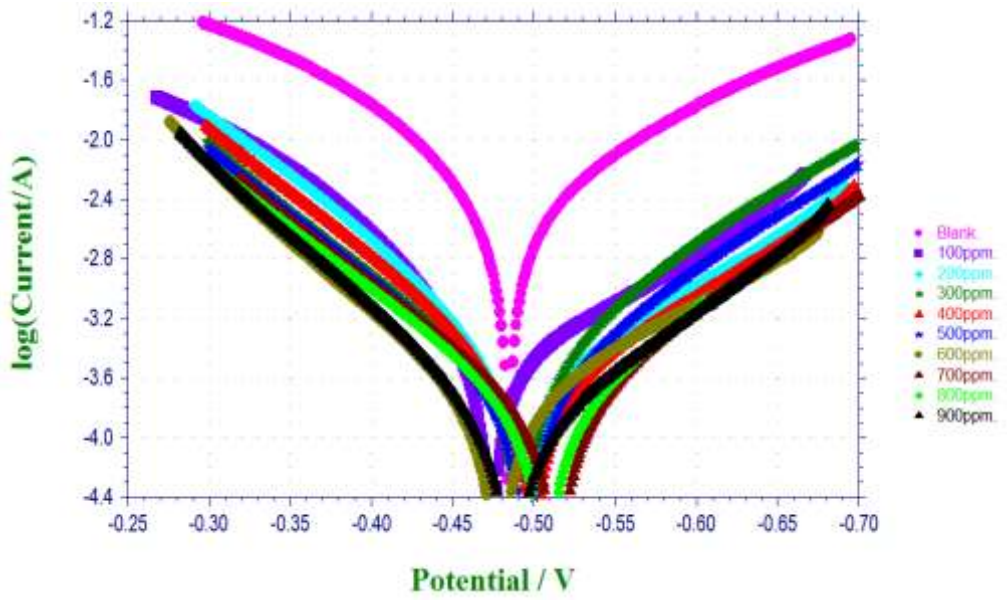

Figure 6.
Potentiodynamic polarization curves for the corrosion of mild steel in 1M HCl in the absence and presence of different concentrations of MSPP at303K.

Table 3. Potentiodynamic Polarization parameters for corrosion of mild steel in 1M HCl in absence and presence of various concentrations of MSPP at room temperature(303K).

Conc. of MSPP (ppm)	Ecorr (V/SCE)	ba (mV dec^{-1})	bc (mV dec^{-1})	Icorr (mA/cm^{-2})	Inhibition efficiency (%)
Blank	-0.484	72.85	65.83	3.981	-
100	-0.474	93.76	63.29	0.4314	89.16
200	-0.493	97.14	65.69	0.2698	93.22
300	-0.492	87.55	85.58	0.2371	94.04
400	-0.499	93.39	68.43	0.2123	94.67
500	-0.495	89.9	82.36	0.1924	95.17
600	-0.478	93.49	61.17	0.1602	95.98
700	-0.514	84.76	82.53	0.1442	96.38
800	-0.507	85.96	89.35	0.1322	96.68
900	-0.487	98.48	78.85	0.1049	97.36

3.2.3. AC impedance spectroscopy studies

Effect of inhibitor concentration on the corrosion of mild steel in 1M HCl solution at 303 K is presented in Fig 7a. It is observed from this figure that all impedance spectra exhibit clearly shows semicircle shaped Nyquist plots with increasing radii with increase in concentration of the inhibitors. The value of R_{ct} is a measure of the electron transfer across the surface and is inversely proportional to corrosion rate. The semicircle indicates the formation of a barrier on the surface and a charge transfer process mainly controlling the corrosion of mild steel. Fig7 b represents the equivalent circuit design used to fit the experimental data of AC impedance for 1M hydrochloric acid in the absence and presence of inhibitor. The inhibition efficiency of MSPP can be calculated using the following formula (6).

$$IE\% = \frac{R_{ct(inh)} - R_{ct(b)}}{R_{ct(inh)}} X100 \qquad (6)$$

Where $R_{ct(inh)}$ and $R_{ct(b)}$ are the charge-transfer resistance with and without inhibitor for mild steel in1M HCl, respectively.

The proposed model with circuit elements for the obtained data include the proposed models successfully describe the phenomenon occurring in the studied system. Table 4 presents the charge transfer resistance (R_{ct}), double layer capacitance (C_{dl}) and inhibition efficiency (%). The C_{dl} values decrease while R_{ct} values increase with increasing inhibitor concentration [24]. The highest R_{ct} (270.92 Ωcm^2) have been found at an optimum concentration (900 ppm). The increase in R_{ct} values is caused by adsorption of inhibitors, indicating that the exposed area for corrosion medium is decreased. On the other hand, a decrease in C_{dl} value suggests that the MSPP molecule due to the adsorption of inhibitor form an adherent film on the metal surface and suggests that the coverage of the metal surface with this film increases the double layer thickness. The maximum inhibition efficiency is found to be 97.92% in 1M HCl for 900 ppm MSPP. These AC impedance measurements are reasonably in good agreement and run parallel with those obtained from weight loss and potentiodynamic polarization measurements.

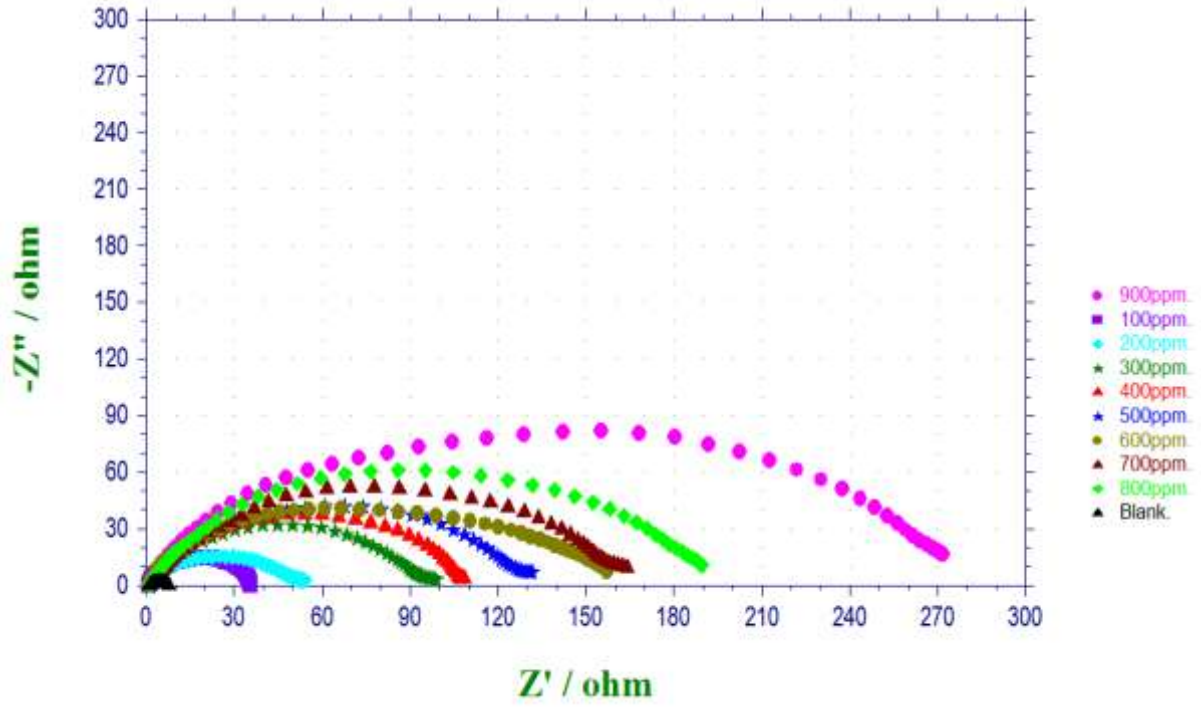

Figure 7a. AC impedance curves (Nyquist plot) for mild steel in the absence and presence of various concentrations of MSPP in 1M HCl at 303K.

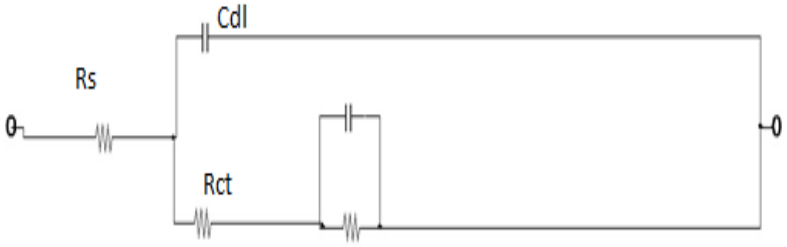

Figure 7b. The electrochemical equivalent circuit used to fit the impedance measurements.

From the Bode phase angle plots it is clear that the measured impedance plot is in accordance with that calculated by the used equivalent circuit model at its open potential Capacitive loop shifted along the real impedance (Zre axis) axis in the high frequency (HF) range and an inductive loop in the lower frequency (LF) range on the other hand, one time constant was observed in the Bode diagram. As seen from Fig.8a&b, the increase of absolute impedance at low frequencies in Bode plot confirms the higher protection with the increasing in inhibitors concentration [25]. These indicate that the corrosion rate reduced in presence of inhibitor and continued to decrease on increasing the concentration of inhibitor.

Table 4. Impedance parameters for the corrosion of mild steel in 1 M HCl containing different concentrations of the MSPP at 303K.

Conc of MSPP (ppm)	R_{ct} (Ω cm^2)	C_{dl} (μF /cm^2)	Inhibition efficiency (%)
Blank	5.64	284.69	-
100	45.48	39.44	87.59
200	52.22	35.55	89.19
300	97.94	20.9	94.24
400	107.59	17.93	94.76
500	130.71	16.82	95.68
600	156.08	16.08	96.38
700	163.07	12.94	96.54
800	188.62	11.44	97.01
900	270.92	8.25	97.92

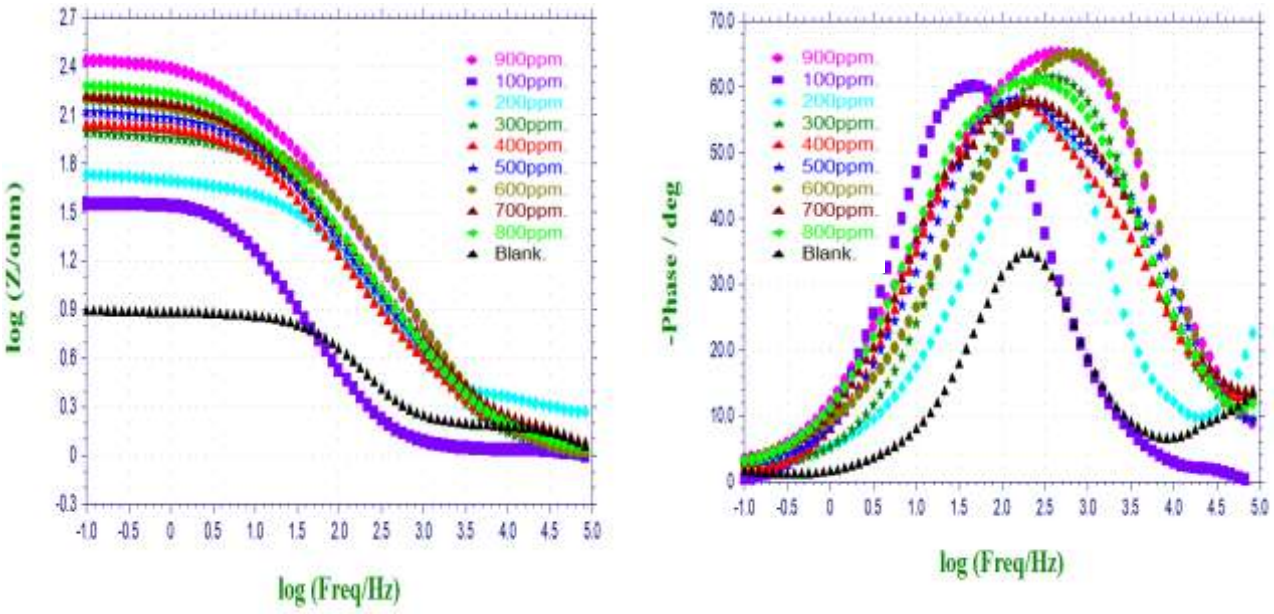

a) **b)**

Figure 8. The Bode plots for mild steel in1M HCl solution in the absence and presence of different concentrations of MSPP.

3.3. Thermodynamic parameters

The thermodynamic activation parameters such as energy of activation E_a, enthalpy of activation (ΔH°) and entropy of activation (ΔS°) for mild steel corrosion in 1M HCl without and with various concentrations of MSPP at 303, 313, 323 and 333K were calculated from an Arrhenius plot (7) and transition state equations (8)

$$\log CR = \frac{-Ea}{2.303RT} + logA \quad (7)$$

$$CR = \frac{RT}{Nh} exp\left(\frac{\Delta S^{\circ}}{R}\right) exp\left(-\frac{\Delta H^{\circ}}{RT}\right) \quad (8)$$

where N is the Avogadro's number, h is the Planck's constant, CR is the corrosion rate , R is the universal gas constant, T is the absolute temperature, ΔH° the enthalpy of activation and $\Delta S^{\circ}$the entropy of activation. Plots of log CR versus 1000/T for blank and various concentration of inhibitor are shown in fig 9. Ea is calculated from the slope of the line, and Plots of log CR/T versus 1000/T was shown in fig 10 straight line is obtained from ΔH° and ΔS° are calculated from the slope and intercepts and the values are presented in Table 5. The positive sign of the enthalpies ΔH reflect the endothermic nature of the mild steel dissolution process. [26]

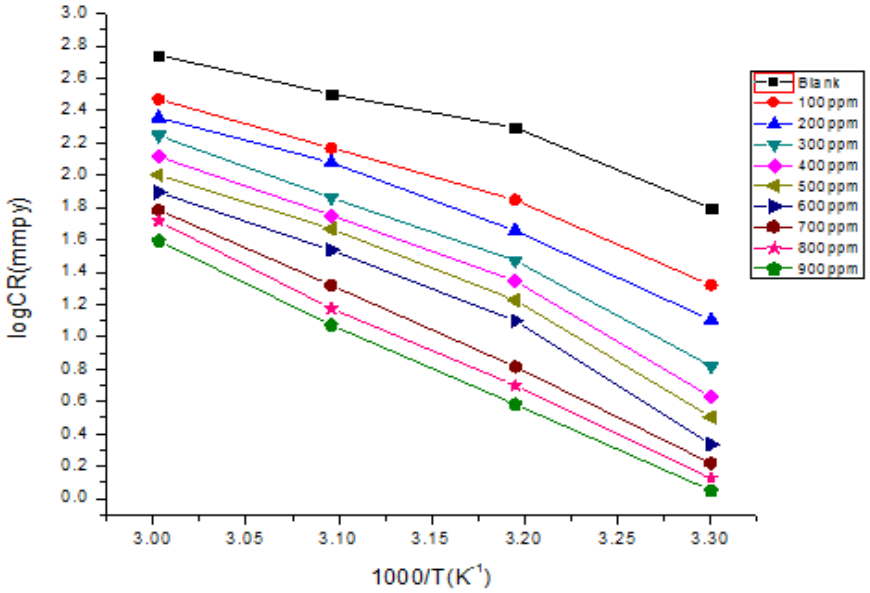

Figure 9. Arrhenius plots of log CR versus 1000/T for mild steel corrosion in 1M HCl in the absence and presence of MSPP.

In the presence of MSPP, the increase of ΔS° reveals that an increase in disordering takes place on going from reactants to the activated complex [27]. The increase in apparent activation energy for the mild steel dissolution in inhibited solution may be interpreted as physical adsorption that occuring in the first stage. Activation energy was found to be 59.22 KJ mol^{-1} in the absence of the MSPP and increases to 188.40 $KJmol^{-1}$in the presence of MSPP at 900 ppm which shows that the adsorbed organic inhibitor has provided a physical barrier to the change and mass transfer, leading to reduction in corrosion rate. Arrhenius factor also reduces with increase in temperature that can be referred to the decrease in the corrosion rate of mild steel with increase in an optimum concentration of inhibitor upto 900 ppm.

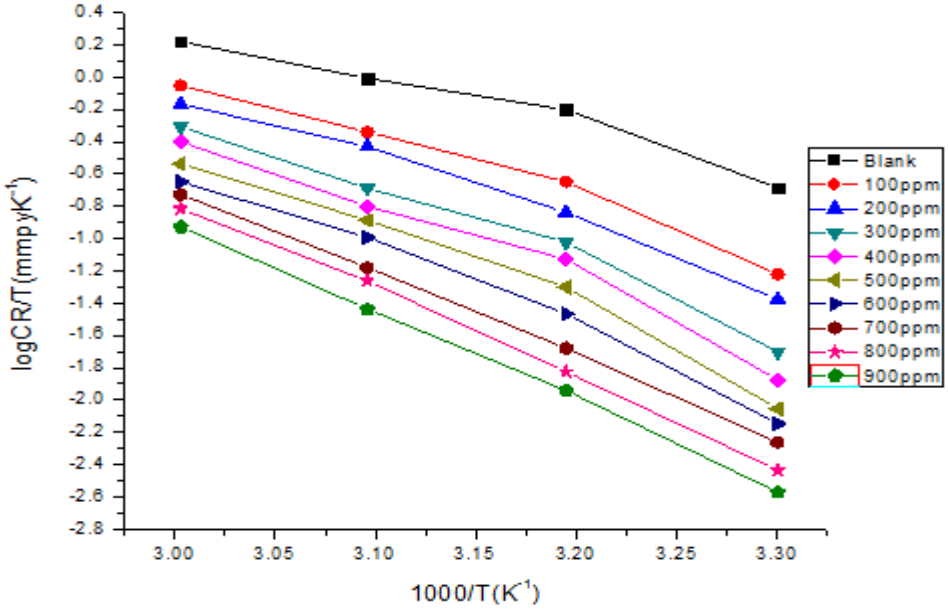

Figure 10: Transition state plots of log CR/T versus 1000/T for mild steel corrosion in 1M HCl absence and presence of MSPP.

Table 5. Activation parameters of mild steel corrosion in 1 M HCl without and with MSPP

Conc of MSPP (ppm)	Ea ($KJmol^{-1}$)	ΔH° ($KJmol^{-1}$)	ΔS° ($Jmol^{-1} K^{-1}$)	$-(\Delta G^{\circ})$			
				303K	313K	323K	333K
Blank	59.22	106.7	-183.1	-	-	-	-
100	96.79	139.6	-180.6	24.49	22.32	21.9	21.2
200	98.71	147.7	-180	24.96	23.41	22.95	22.64
300	101.45	166.6	-178.6	25.3	23.62	23.53	23.22
400	102.54	180.2	-177.6	25.48	23.79	23.77	23.48
500	106.29	181.5	-177.5	25.58	23.96	23.92	23.65
600	109.56	192.5	-176.7	25.59	24.1	24	23.71
700	111.99	212.5	-175	26.09	24.38	24.07	23.82
800	114.13	217.5	-174.8	26.57	25.65	25.42	23.95
900	188.4	221.4	-174.2	27.35	26.26	25.7	24.04

Table 5 shows that the values of ΔG°_{ads} calculated from equation (6). The values of AG°_{ads} around -20 $kJmol^{-1}$ or lower are consistent with electrostatic interaction between charged molecules and a charged metal (which indicates physisorption), those around -40 KJ mol^{-1} or higher involve charge sharing or transfer from the inhibitor molecules to the metal surface to form a co-ordinate type of bond (which indicates chemisorption). The negative values of ΔG°_{ads} ranging from -27.35 to-24.04 kJ/mol indicate that the adsorption of inhibitor is spontaneous and also chemically adsorbed on mild steel in 1MHCl. The unshared electron pairs in nitrogen, oxygen and sulphur atoms may interact with d-orbital of mild steel to provide a protective Physisorbed film [28].

.

$$\Delta G_{ads} = -RT\ln(55.5K_{ads}) \quad (6)$$

3.4. Adsorption Isotherm

The mode and interaction degree between an inhibitor and a metallic surface have been widely studied with the application of adsorption isotherms. The most frequently used adsorption isotherms are Langmuir, Temkin, Frumkin and Freundlich isotherms. Langmuir adsorption isotherm is represented by following equation.

$$\frac{C}{\theta} = \frac{1}{K} + C \quad (7)$$

In order to obtain the adsorption isotherm, the degrees of surface coverage (Θ) were calculated for various concentrations of the inhibitor from the weight loss data.

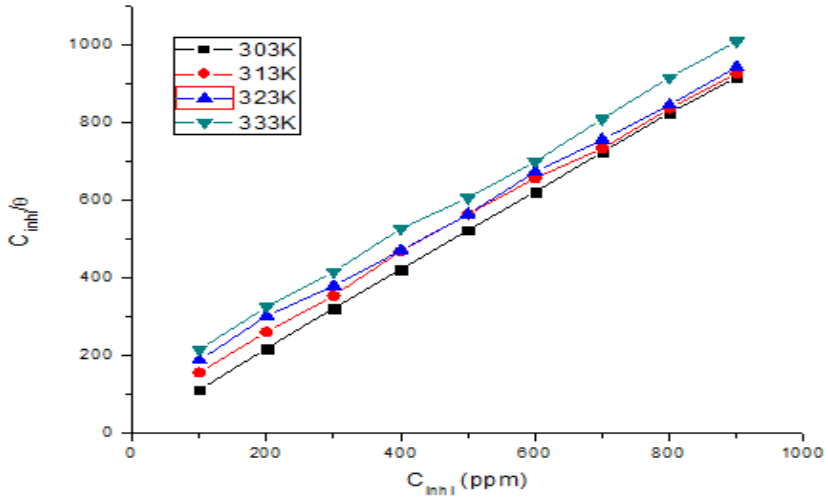

Figure 11. Langmuir adsorption isotherm plot for mild steel in 1M HCl with MSPP.

Fig 11: A plot of C/Θ versus C for various temperature and the values of R^2 and slope are listed in the table 6 used to describe the adsorption process that is based on assumption all the adsorption sites are equal denoting the probability of adsorption is same everywhere. There is a monolayer adsorption and it cannot proceed beyond monolayer. There is no interaction between the adsorption molecule and the adsorption process is independent of the neighboring occupied sites [29]. The slope of the straight line obtained from the isotherm for all the temperature is nearly 1.13, greater than 1 which suggests that 1 molecule of MSPP occupies more than 1 site approximately 1.13 adsorption site on the mild steel. The values of θ were then plotted to fit the most suitable model of adsorption [30-31].

Table 6. Adsorption factors in the presence of MSPP on mild steel in 1M HCl at different temperature.

Temperature (K)	R^2	slope	K_{ads}	-ΔG
303	0.9998	1.118	4546	24.02
313	0.9956	1.136	1818	22.53
323	0.9856	1.129	1533	21.70
333	0.9763	1.176	759	20.36

The values of ΔG_{ads} are given in Table 6. Inspection of these table shows that the higher values of K_{ads} negative sign of ΔG indicates that MSPP is strongly adsorbed on the surface of the mild steel mean better inhibition efficiency of a given inhibitor, strong electric interaction between the double layer existing at the phase boundary and the adsorbed species. The value of K_{ads} and ΔG decreases with increasing in temperature. Small values of K_{ads}, however, compromise that such interactions are weaker, denoting that the adsorbed species are easily removable by the solvent molecules from the surface [32].The decrease in the inhibition efficiency with increase in temperature may be attributed to the increase in the solubility of the protective film or the reaction products precipitated on the surface of the metal that might otherwise inhibit the reaction [33-34].

3.5. UV-Visible spectroscopy

The surfaces of corroded and corrosion inhibited mild steel specimens were examined by absorbance studies in the region 200- 800 nm using (mode: Lambda 35) Perkin-Elmer UV-Visible spectrophotometer. The corrosion inhibition of mild steel in 1M HCl in the presence of inhibitor may be due to the formation of thin film on the metal surface is shown in the Fig12. Mild steel was gradually decreases for the specimen dipped in 1M HCl solution. This observation reveals that the change in surface characteristic is due to the corrosion of mild steel. After corrosion, it can be observed that, in the presence of MSPP corresponding to six absorption peaks observed at the same time, The absorbance value 0.52 shifts to 3.5 It is clearly seen that the bands are shifted to higher frequency region suggesting the interaction between MSPP and Fe^{2+} ions in the solution [35]. This indicates that the nitrogen and sulphur groups are tightly held up in the complex with iron. This changes of adsorption peaks clearly indicates that the strong binding between the inhibitor molecules and the ions in the metal surface. These experimental findings provide a strong evidence for the formation of complex between MSPP and Fe^{2+} UV-visible observation confirms the formation of a protective film of metal inhibitor complex on the metal surface.

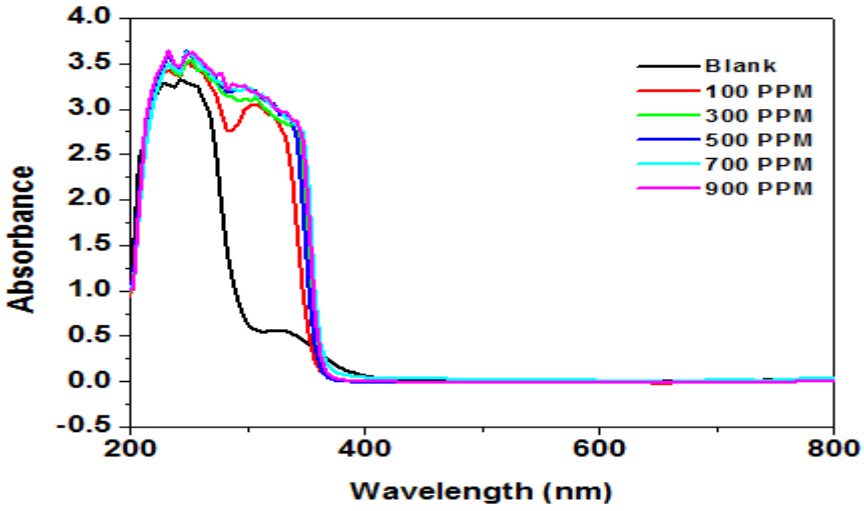

Figure 12. UV-Visible spectra of mild steel in 1M HCl in the absence and presence of MSPP.

3.6. FT-IR Analyses

Fig13a and 13b shows the FT-IR for spectra mild steel in 1M HCl in the absence and presence of MSPP. The peak appeared in the region of 3432.28cm^{-1}, 2829.80 cm^{-1}, 1592.98 cm^{-1}, 1358.13 cm^{-1}, 773.95 cm^{-1}are shifted to 3434.53 cm^{-1}, 2831.05cm^{-1}, 1592.85 cm^{-1}, 1360.39 cm^{-1}, 775.23 cm^{-1}. This is due to the interaction of sulphur, nitrogen, oxygen atoms present in MSPP with Fe in mild steel thereby Fe-MSPP complex is formed. It reduces the dissolution of mild steel surface.

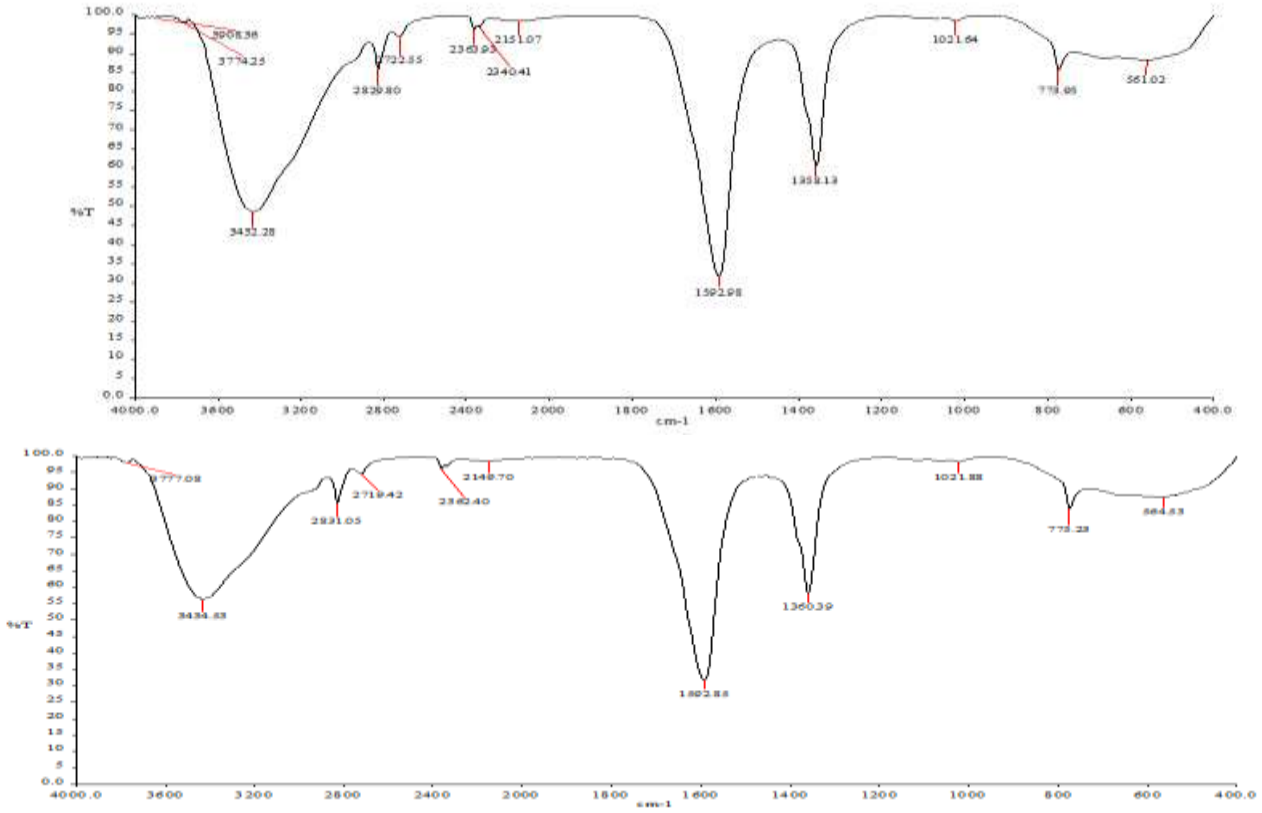

Figure 13a**.** FT-IR spectrum of mild steel in 1M HCl without MSPP
Figure 13 b FT-IR spectrum of mild steel in 1M HCl with MSP

B

3.7 Surface Analyses

3.7.1 Scanning Electron Microscopy (SEM) Analysis

Fig.14 shows the SEM images of mild steel surface immersed in 1 M HCl at 3hr in the absence and presence of MSPP for 900 ppm. The SEM image of mild steel in absence of MSPP Fig (14A) shows that the deterioration of metal surface due to the attack of corrosive solution found to be corroded seriously with the formation of many cracks and pits, This observation indicates that corrosion rate is reduced to a very low value in the presence of the inhibitor [36]. While a layer of closely packed film is obtained in Fig(14B) and the surface is smooth and free from pits. The chemical reaction between the metal surface and the inhibitor containing nitrogen, sulphur and oxygen-rich of electronic pairs as well as possession of double bonds and these electrons combine with the metal by transfer of electrons from the ligand to the unoccupied d-orbitals of the metal and the formation of coordination bonds, confirmed the absorbed protective film on the mild steel surface and the uniform growth of organic compound on the metal surface, leads to greater corrosion protection efficiency.

(b)

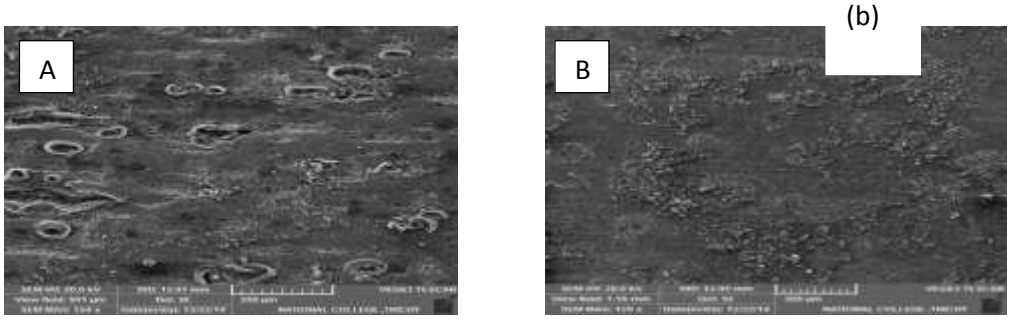

Figure 14**.** Surface characterization by SEM for mild steel in 1M HCl in the (a) absence and (b) presence of MSPP.

3.7.2. Atomic force Microscopy (AFM)

The surface morphology and microstructure were analysis. AFM has become a new choice to study the influence of inhibitor on the generation and the progress of the corrosion at the metal/solution interface. The mild steel surface exposed to 1M HCl in the absence and presence of inhibitor for 3 h.

The 2D and 3D AFM images were taken at room temperature in the first position range of 0.05µm to 0.65µm, and the average roughness of blank mild steel surface and second position range from 0.05µm to 0.90 µm in absence of inhibitor for 1 M HCl solution Fig(15A). The mild steel surface severely damaged and cracks due to acid attack are clearly evident in the photograph.

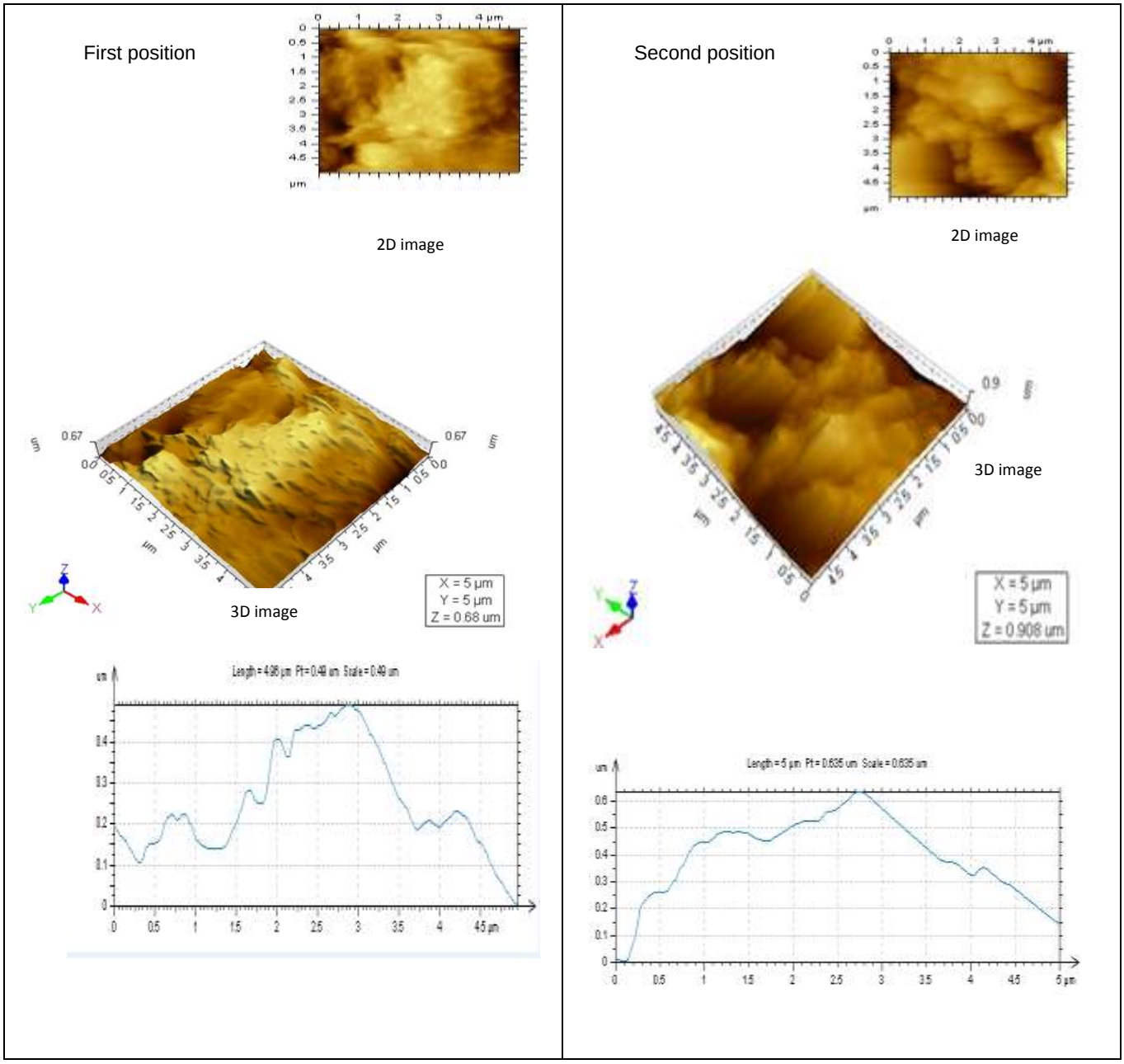

Figure 15 A. 2D and 3D AFM images of mild steel immersion in 1M HCl without MSPP.

However, in presence of optimum concentration of MSPP of 900 ppm the average roughness is reduced to first position from 0.025µm and 0.4µm, and second position 0.025µm and 0.45µm respectively Fig(15B). A smoother layer with clearly different morphology is seen as a result of the formation of a good protective layer by the adsorbed inhibitor molecules over the surface of mild steel [37]. AFM data for mild steel is given in table 7.

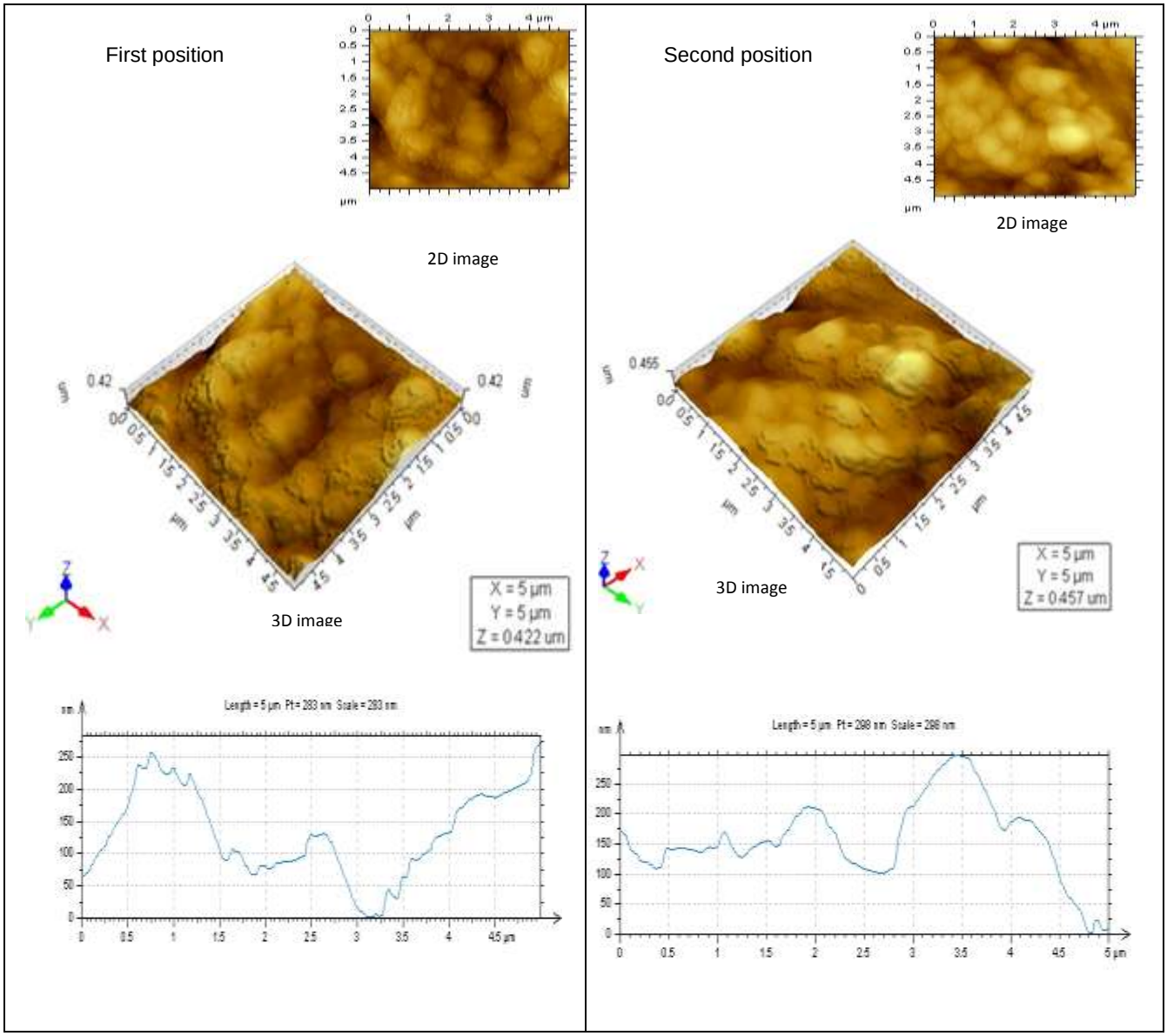

Figure 15 B. 2D and 3D AFM images of mild steel immersion in 1M HCl with MSPP.

Table 7. AFM parameters data for mild steel in the absence and presence of an optimum Concentration 900 ppm of inhibitor in 1M HCl.

Sample	Root mean Square roughness (µm)	Average roughness (µm)	Maximum peak height (µm)	Maximum surface height (µm)
1M HCl without MSPP (1st position)	0.129	0.107	0.305	0.68
1M HCl with MSPP (1st position)	0.0603	0.0489	0.245	0.422
1M HCl without MSPP (2st position)	0.126	0.099	0.494	0.908
1M HCl with MSPP (2st position)	0.0731	0.0608	0.227	0.457

3.7.3 X- ray diffraction analysis

X-ray diffraction studies are used to determine film formation of mild steel in immersed in 1 M HCl in the absence and presence MSPP shown in Fig.16 (a,b) respectively. The peak appear at 2θ= 44.71°, 65.04°, and 82.58 (Fig. 16a) suggested the presence iron oxide (Fe_2O_3) and very small amount of brown film, which led to corrosion. [38]. The XRD pattern of the surface of the mild steel immersed in the 1M HCl solution containing 800 ppm of MSPP is shown in (Fig.16b). The iron peaks appear at 2θ = 44.69, 64.93 and 82.31. It is observed that the peaks due to oxides of iron such as Fe_3O_4 and FeOOH are found to be absent. The formation of adsorbed protective film on the surface of mild steel in the presence of MSPP is clearly reflected from these observations.

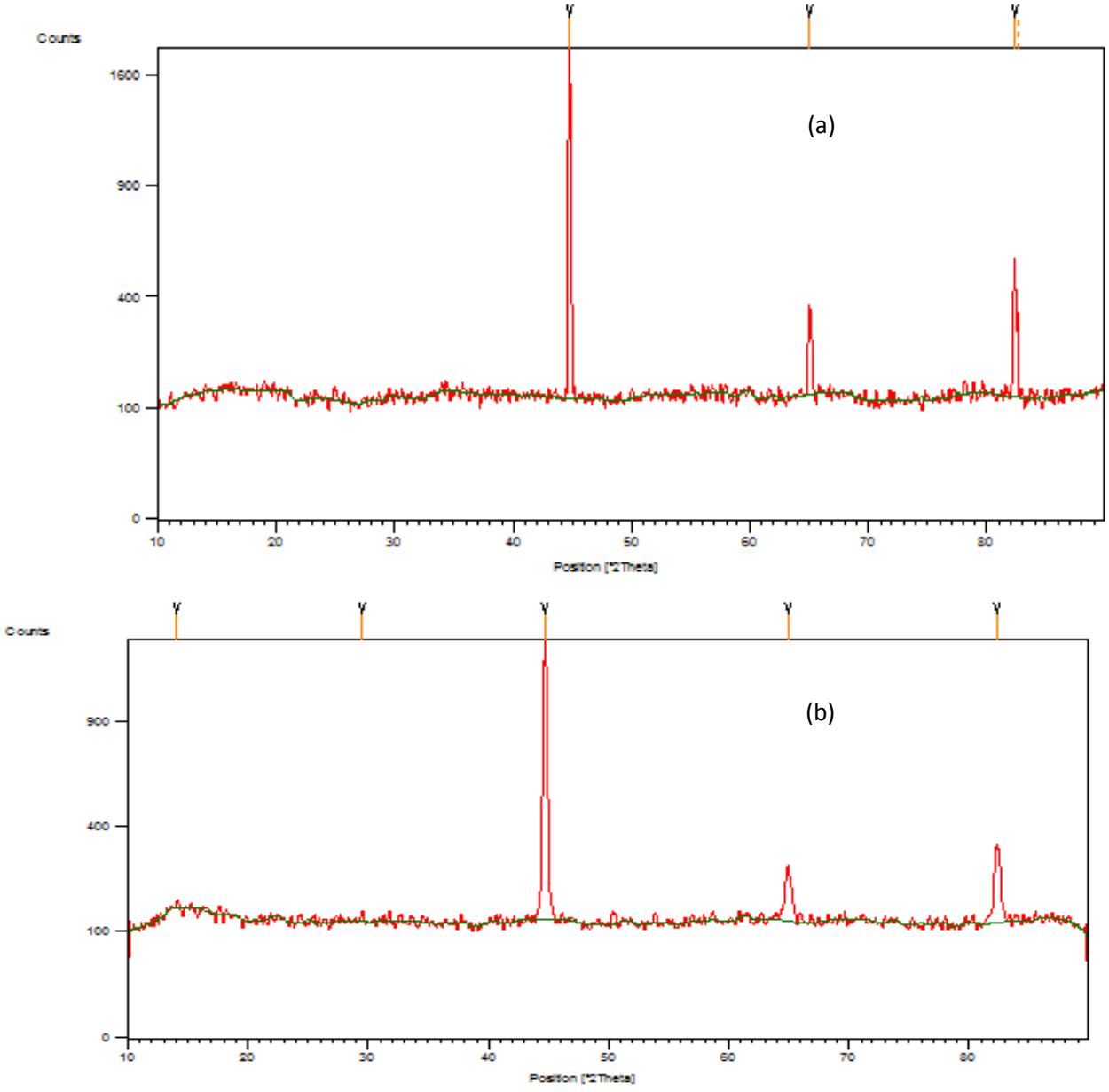

Figure16: XRD spectrum of mild steel corrosion in the (a) absence and (b) presence of MSPP.

3.8. Quantum chemical calculations

Quantum chemical calculations for the adsorption and inhibition mechanism that relate the Density functional theory (DFT) has been used to analyse the characteristics of the inhibitor/ surface mechanism and to describe the structural MSPP of the inhibitor in the corrosion process. **Fig17 (a-d)** represent the optimized molecular structure, E_{HOMO} , E_{LUMO} and MEP of MSPP.

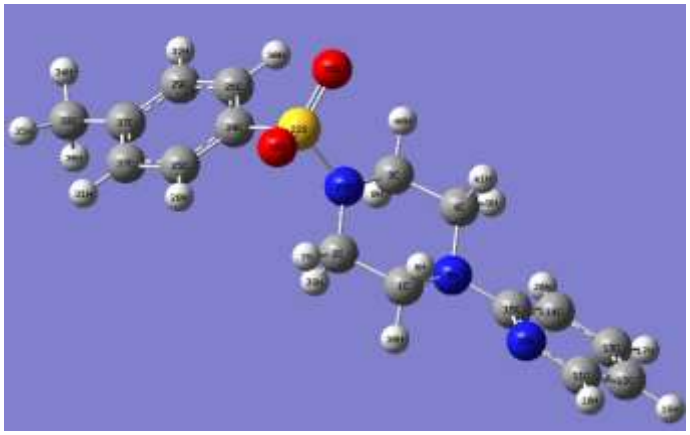

Figure 17a. Optimized molecular structure of MSPP.

$$\eta = \frac{E_{LUMO} - E_{HOMO}}{2} \quad (8)$$

$$\sigma = \frac{1}{\eta} \quad (9)$$

$$\chi = -1/2\ (E_{HOMO}+E_{LUMO}) \quad (10)$$

$$\omega = \mu^2 /2\eta \quad (11)$$

The 3D structure and frontier molecular orbital calculated at density functional theory (DFT) level of approximation. Some of the quantum chemical indices such as dipole moment, E_{HOMO} (-0.32768), E_{LUMO} (-0.0235), energy gap (ΔE), chemical hardness (η), softness (σ), absolute electronegativity (χ) and electrophilicity (ω) of the MSPP models were calculated and given in table 8. It has been reported in the literature [39] that, higher values of E_{HOMO} is an indication of the greater ease of donating electrons to the unoccupied d orbital of metal, and the higher the corrosion inhibition efficiency.

Table 8. The calculated quantum chemical parameters for the inhibitor obtained using DFT at the B3LYP/6-311G (d,p) basis set and semi empirical (PM6) method

Inhibitor	E Homo (ev)	E Lumo (ev)	ΔE (ev)	Hardness (η)	softness (σ)	χ	ω
MSPP	-0.32768	-0.0235	0.30418	0.15209	6.57505	0.1756	1.8964

Theoretical dipole moment data of compound				
Inhibitor	μ_x (D)	μ_y (D)	μ_z (D)	μ_{tot} (D)
MSPP	0.1056	-2.0870	-0.3519	2.1138

In addition, the lower the E_{LUMO} energy, the easier the acceptance of electrons from metal surface, as the E_{LUMO}-E_{HOMO} energy gap decreased and the efficiency of inhibitor improved. Moreover, unoccupied d orbitals of Fe atom can accept electrons from the inhibitor molecule to form a coordinate bond while the inhibitor molecule can accept electrons from Fe atom with its anti-bonding orbitals to form back-donating bond. In the present study MSPP has higher σ value (7.12555) and lower η value (0.14034). Normally, the inhibitor with the least value of global hardness η and highest value of global softness σ is expected to have the highest inhibition efficiency. The increasing values of μ given in table may facilitate adsorption (and therefore inhibition) by influencing the transport process through the adsorbed layer.

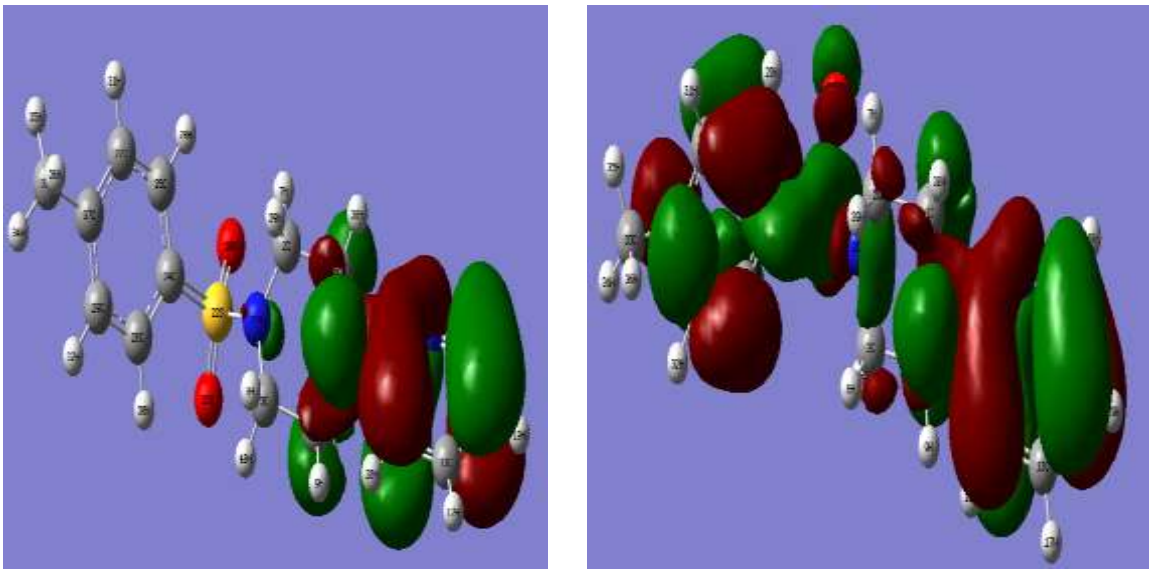

(b) (c)

HOMO LUMO

Figure 17b/c. Frontier molecule orbital density distributions of the MSPP: HOMO and LUMO

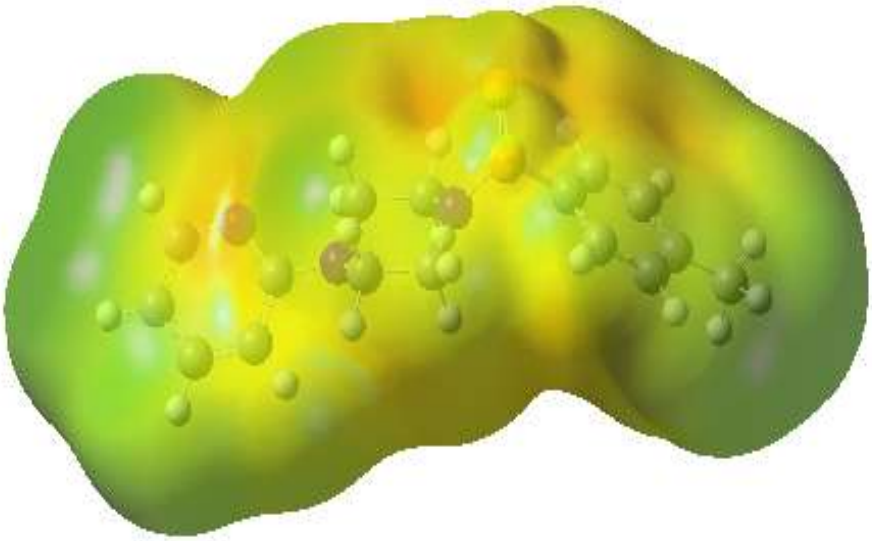

Figure 17d. Molecular electrostatic potential **(**MEP) for MSPP molecule.

Molecular electrostatic potential MEP were calculated for all the optimized structures Fig.17(d). In all the structures the negative Charge density is localized on the oxygen atom, sulphur and nitrogen atoms of the MSPP indicating a high ability in metal coordination.

The non-linear optical parameters such as dipole moment (2.1138), polarizability, anisotropy of polarizability and first order hyperpolarizability of selected compound were calculated using B3LYP level with 6-311G (d, p) basis set and semi empirical (PM6) method. The numerical values of the above mentioned parameters are listed in Tables (11a,11b,12), in the presence of an external field (E), the energy of the system is a function of the electric field. First hyperpolarizability is a third-rank tensor that can be described by a 3 X 3 X 3 matrix. The 27 components of the 3D matrix can be reduced to 10 components due to the Kleinman symmetry. The components of hyper polarizability are defined as the coefficients in the Taylor series expansion of energy in an external electric field.

The polarizability and hyperpolarizability tensors (α_{xx}, α_{xy}, α_{yy}, α_{xz}, α_{yz}, α_{zz} and β_{xxx}, β_{xxy}, β_{xyy}, β_{yyy}, β_{xxz}, β_{xyz}, β_{yyz}, β_{xzz}, β_{yzz}, β_{zzz}) can be obtained by a frequency job output file of Gaussian software.

However, the polarizability and hyperpolarizability values of Gaussian output are in atomic units (a.u) so they have been converted into electrostatic units (e.s.u) (for α: 1a.u. = 0.1482 $\times 10^{-24}$ e.s.u, for β:1 a.u. = 8.6393 $\times 10^{-33}$ e.s.u).The total static dipole moment (μ), mean polarizability (α_{tot}), anisotropy polarizability (Δα) and the average value of the first hyperpolarizability (β) can be calculated using the following equations,

$$\mu = (\mu_x^2 + \mu_y^2 + \mu_z^2)^{1/2}$$

$$\alpha_{tot} = \frac{1}{3}(\alpha_{xx} + \alpha_{yy} + \alpha_{zz})$$

$$\langle\beta_{tot}\rangle = [(\beta_{xxx} + \beta_{xyy} + \beta_{xzz})^2 + (\beta_{yyy} + \beta_{yzz} + \beta_{yxx})^2 + (\beta_{zzz} + \beta_{zxx} + \beta_{zyy})^2]^{\frac{1}{2}}$$

Urea is one of the prototypical molecules used in the study of the NLO properties of molecular structure. Therefore, it is used frequently as a threshold values for comparative purposes. (μ,α and β of urea are 1.3732 Debye, 3.8351x10-24 esu and 3.7347x10-31 esu respectively). More active NLO properties are predicted for molecules having greater dipole moment, molecular polarizability and hyper polarizability than urea.

Theoretical dipole moment, molecular polarizability and hyper polarizability of compound and complexes are shown in tables 9.

Table 9. Theoretical polarizability and hyperpolarizability data of compound

polarizability (MSPP)		Hyperpolarizability (MSPP)	
α_{xx} (a.u)	310.495	β_{xxx} (a.u)	-844.09
α_{xy} (a.u)	-4.649	β_{yxx} (a.u)	216.411
α_{yy} (a.u)	161.509	β_{xyy} (a.u)	-86.925
α_{xz} (a.u)	2.499	β_{yyy} (a.u)	-85.8066
α_{yz} (a.u)	-0.395	β_{zxx} (a.u)	148.5317
α_{zz} (a.u)	97.584	β_{zyy} (a.u)	23.8121
α_{tot} (e.s.u)	2.8137×10^{-23}	β_{xzz} (a.u)	46.3204
		β_{yzz} (a.u)	-45.049
Δα (e.s.u)	2.8076×10^{-23}	β_{zzz} (a.u)	-58.4733
		β_{tot} (e.s.u)	6.2382×10^{-30}

The dipole moment, polarizability and hyperpolarizability of MSPP are greater than those of urea. This hyperpolarizability value is about 16.7 times greater than those of urea. Therefore this MSPP can be used as an effective NLO material.

3.8.1. Mulliken atomic charges and Fukui functions

The use of Mulliken population analysis to estimate the adsorption centers of MSPP has been widely reported and it is mostly used for the calculation of charge distribution over the whole skeleton of the molecule. It has been reported

that as the Mulliken charges of the adsorbed centre become more negative, which could offer electrons to the mild steel surface to form a coordinate bond. It could be readily observed that oxygen, nitrogen atoms and the benzene ring had higher charge densities and might form the adsorption centers. From the Table 10, it is clear that nitrogen, oxygen and sulphur atoms have high charge densities. Thus, the bond with the metal from sulfur will be easily formed, rather than N or C atoms. Several authors agree that the more negatively charged heteroatom is the merrier is its ability to adsorb on the metal surface, through a donor-acceptor type reaction.

Table 10. Mulliken atomic charges for MSPP compound

Atom No	Mulliken charge	Atom No	Mulliken charge	Atom No	Mulliken charge	Atom No	Mulliken charge
1 C	0.190013	11C	0.087804	21 N	-1.313672	32 H	0.130526
2 C	0.285516	12 C	-0.351049	22 S	3.324163	33 C	-0.105132
3 C	0.29708	13 C	0.139921	23 O	-1.011807	34 H	0.050563
4 C	0.186809	14 C	-0.384646	24 C	-1.011827	35 H	0.050922
5 N	-0.720879	15 C	0.583227	25 C	0.115497	36 H	0.04499
6 H	-0.005825	16 N	-0.370602	26 C	0.115026	37 C	0.252167
7 H	0.051073	17 H	0.123991	27 C	-0.336319	38 H	0.045526
8 H	-0.008438	18 H	0.144945	28 H	0.135467	39 H	-0.00853
9 H	0.027778	19 H	0.157831	29 C	-0.337136	40 H	0.050951
10 O	-1.008291	20 H	0.134456	30 H	0.135621	41 H	-0.018838
				31 H	0.131159		

3.9. Mechanism of Inhibition

The studied compound shows good inhibition efficiencies towards corrosion of mild steel in 1M HCl by MSPP that can be made clear on the basis of molecular adsorption between inhibitor and Mild steel is donor-acceptor type. Organic compounds adsorbed on the metal surface by electrostatic interaction between the charged molecule and charged metal, interaction of π electron with the metal and interaction of unshared pair of electrons in the molecule with metal shown in Fig(18 a,b) [40]. It is well known that mild steel has coordinate affinity toward sulphur, nitrogen, and oxygen-bearing ligand; hence, adsorption on mild steel can be attributed to coordination through the -NH group. Thus, the protonated species adsorbed on the cathodic sites of the mild steel and decrease the evolution of hydrogen. MSPP adsorbed on anodic sites through lone pair of electrons of nitrogen atom and π electrons of aromatic ring and hence, anodic dissolution of mild steel is decreased .

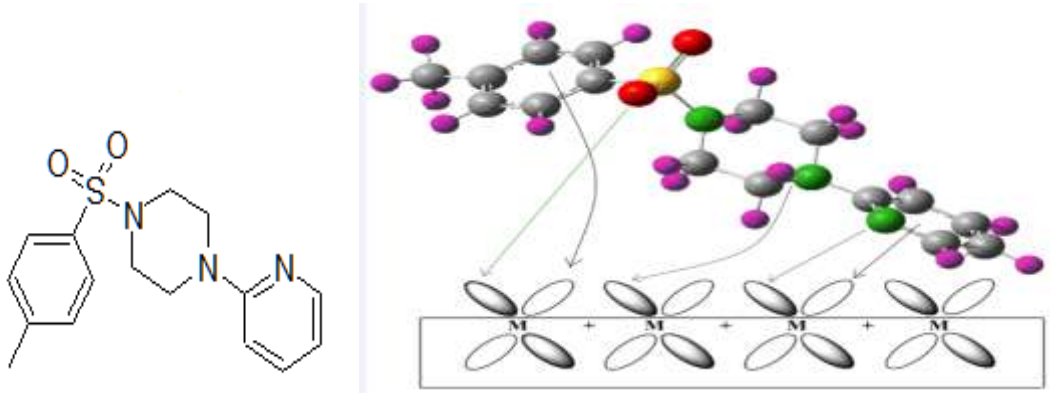

(a) (b)

Interaction with the aromatic π-electrons
Interaction with the p-electrons

Figure 18. (a) Chemical structure of MSPP and (b) interaction of MSPP sites with the mild steel surface.

4. CONCLUSIONS

1. The structure of the newly synthesized MSPP was confirmed using ^{1}H NMR, ^{13}C NMR and FT-IR spectroscopy. The relatively molecular weight of the compound was confirmed by mass spectrum. The TGA and DSC curves provided previously unreported information about the thermal stability and thermal decomposition of MSPP.

2. The investigated MSPP are found to be an effective inhibitor for mild steel corrosion in 1 M HCl solution. The optimum concentration of the inhibitor was found to be 900 ppm for the maximum inhibition efficiency of 99.75%. Polarization measurements indicate that MSPP acts as mixed type inhibitor.

3. Thermodynamic parameters show that the adsorption of MSPP follows Langmuir adsorption isotherm. XRD, SEM , AFM and micrographs indicated the formation of very good protective film on the MS surface after 3 h immersion in the presence of MSPP in 1 M HCl.

4. Quantum chemical studies by DFT at the B3LYP/6-31G (d) level of theory were correlated to the inhibitive effect of MSPP.

5. The results obtained from weight loss, EIS and polarization curves were in good agreement.

REFERENCES

1. Ahmed, A., Al- Amiery,, Abdul Amir H. Kadhum,, M. Abdul Hameed, Alobaidy., Abu bakar mohamad., pua soh Hoon., 2014. Novel Corrosion Inhibitor for Mild Steel in HCl. Mater. 7, 662.
2. Abdallah, M., El Defrawy, A. M., Zaafaranya, I.M., Sobhi, M., Elwahy, A.H.M., Shaaban, M.R., 2014. Inhibition Effects and Theoretical Studies of Synthesized Novel Bisaminothiazole Derivatives as Corrosion Inhibitors for Carbon Steel in Sulphuric Acid Solutions. Int. J. Electrochem. Sci. 9, 2186.
3. Adallal, M., Helal, E.A., Fouda, A.S., 2006. Aminopyrimidine derivatives as inhibitors for corrosion of 1018 carbon steel in nitric acid solution. Corros. Sci. 48,1639.
4. Dubey, A.K., Singh, G., 2007. Corrosion Inhibition of Mild Steel in Sulphuric Acid Solution by Using Polyethylene Glycol Methyl Ether. portuga. Electro. Acta. 25, 221.
5. Ramesh, S., Rajeswari, S., Maruthamuthu, S., 2003. Effect of inhibitors and biocide on corrosion control of mild steel in natural aqueous environment. Mater. letters. 57. 4547.
6. Fouda, A.S., Abdallah. Y.M., Nabil, D., 2014 Dimethyl pyrimidine derivatives as corrosion inhibitors for carbon steel in hydrochloric acid solutions. Int. J. Inno. Resear. Sci. Engg &Tech. 5, 12965.
7. Singh, A. K., Shukla, K.S., Singh, M., Quraishi, M.A., 2011. Inhibitive effect of ceftazidime on corrosion of mild steel in hydrochloric acid solution. Mater. Chem. Phys., 129, 68.
8. Shukla, S. K., Quraishi, M. A., 2010. Cefalexin drug: A new and efficient corrosion inhibitor for mild steel in hydrochloric acid solution. Mater. Chem. Phys. 120, 142.
9. Emregul, K., Atakol, O.C., 2003. Corrosion inhibition of mild steel with Schiff base compounds in 1 M HCl Mater. Chem. Phys., 82 ,188.
10. Lagrenee, M., Mernari, B., Bouanis, M., Traisnel, M., Bentiss, F., 2002. Study of the mechanism and inhibiting efficiency of 3,5-bis(4-methylthiophenyl)-4H-1,2,4-triazole on mild steel corrosion in acidic media. Corros. Sci. 44, 573.
11. Elayyachi, M., El Idrissi, A., Hammouti, B., 2006. New thio-compounds as corrosion inhibitor for steel in 1 M HCl. Corros. Sci. 48, 2470.
12. Ma, H., Song, T., sun, H., Li, X., 2008. Experimental and theoretical elucidation on the inhibition mechanism of 1-methyl-5-mercapto-1,2,3,4-tetrazole self-assembled films on corrosion of iron in 0.5 M H_2SO_4 Solutions. Thin solid films. 516, 1020.

13. El Ashry, E.H., El Nemr, A., Essawy, S.A., Ragab, S., 2008. Corrosion inhibitors part V: QSAR of benzimidazole and 2-substituted derivatives as corrosion inhibitors by using the quantum chemical parameters. Prog. Org. Coat. 61,11.
14. Ju, H., Kai, Z.P, Li, Y., 2008. Aminic nitrogen-bearing polydentate Schiff base compounds as corrosion inhibitors for iron in acidic media: A quantum chemical calculation. Corros. Sci. 50, 865.
15. Hari Kumar, S., Karthikeyan, S., 2012. Inhibition of mild steel corrosion in hydrochloric acid solution by cloxacillin drug. J. Mater. Environ., 3(5), 925.
16. Szyprowski, A.J., 2000. Relationship between chemical structure of imidazoline inhibitors and their effectiveness against hydrogen sulphide corrosion of steels. Britis. Corros. J. 35,155.
17. Granese, S.L., Rosales, B.M., Oviedo, C., Zerbino, J.O. 1992. The inhibition action of heterocyclic nitrogen organic compounds on Fe and steel in HCl media. Corros. Sci. 33,1439.
18. Rajappa, S.K., Venkatesha, T., 2002. New condensation products as corrosion inhibitors for mild steel in hydrochloric acid medium. Indian. J. Eng. Mater. Sci. 9. 213.
19. Mora-Mendoza, J.L., Chacon-Nava, J.G., Zavala-Olivares, G., Gonzalez-Nunez, M.A., Turgoos, S., 2002. Influence of Turbulent Flow on the Localized Corrosion Process of Mild Steel with Inhibited Aqueous Carbon Dioxide Systems. Corros. Eng., 58, 608.
20. Negma, N.A., Elkholy, Y.M., Zahran, M.K., Tawfik, S.M., 2010. Corrosion inhibition efficiency and surface activity of benzothiazol-3-ium cationic Schiff base derivatives in hydrochloric acid. Corros. Sci. 52, 3523.
21. Ben Hmamou, D., Salghi, R., Zarrok, H., Zarrouk, A., Hammouti, B., Mt. El Hezza, M., Bouachrin, M., 2012. Temperature Effects on the Corrosion Inhibition of Carbon Steel in Acidic Solutions by Alizarin Red. Adva. Mate. Corros. 36.
22. ELouadi, Y., Abrigach, F., Bouyanzer, A., Touzani, R., Riant, O., ElMahi, B., El Assyry, A., Radi1, S., Zarrouk, A., Hammouti, B., 2015. Corrosion inhibition of mild steel by new N-heterocyclic compound in 1 M HCl: Experimental and computational study. Der. Pharma. Chemica. 7, 265.
23. El Mehdi, B., Mernari, B., Traisnel, M., Bentis, F., Lagrenee, M., 2003. Synthesis and comparative study of the inhibitive effect of some new triazole derivatives towards corrosion of mild steel in hydrochloric acid solution. Mater. Chem. Phys. 77, 489.
24. Nalini, D., Rajalakshmi, R., Subhashini, S., 2011. Corrosion Inhibition of Mild Steel in Acid Solution by 3,4,5-Trimethoxyphenyl-2-imidazolines. E-J.Chem., 8, 671.
25. Hegazy, M.A., Abdallah, M., Awad, M.K., Rezk, M. 2014. Three novel di-quaternary ammonium salts as corrosion inhibitors for API X65 steel pipeline in acidic solution. Part I: experimental results. Corros. Sci. 81, 54.
26. Guan, N.M., Xueming, L., Fei , L., 2004. Synergistic inhibition between o-phenanthroline and chloride ion on cold rolled steel corrosion in phosphoric acid. Mater. Chem. Phys. 86, 59.
27. Khamis, E., Hosny, A., El-hadary, S., 1995. Thermodynamics Of Mild-Steel Corrosion Inhibition In Phosphoric-Acid By Ethylene Trithiocarbonate. Afinidad. 52, 95.
28. Ramesh saliyan, V., Airody, V.A., 2009. Corrosion inhibition of mild steel in acid media by quinolinyl thiopropanohydrazone. Indian.J.chem.Technol.,16, 162.
29. Abdel-Rehim, S.S., Khaled, K.F., Al-mubarak, N.A., 2011. Corrosion inhibition of iron in hydrochloric acid using pyrazole. Arabian. J. chem. 4, 333.
30. Bockris, J.O.M., Swinkels, D.A.J., 1964. Adsorption of n-Decylamine on Solid Metal Electrodes. J. Electrochem. Sci. 111, 736.
31. Saleh, M.M., Atia, A.J., 2006. Effects of structure of the ionic head of cationic surfactant on its inhibition of acid corrosion of mild steel. Appl. Electrochem., 36, 899.
32. Amin, M.A., Abd El Rehim, S.S., El-Sherbini, E.E.F. Bayoumi, R.S., 2008. Chemical and Electrochemical (AC and DC) Studies on the Corrosion Inhibition of Low Carbon Steel in 1.0 M HCl Solution by Succinic Acid - Temperature Effect, Activation Energies and Thermodynamics of Adsorption. Int. J. Electrochem. Sci. 3, 199.
33. Ebenso, E.E., Hailemichael Alemu, Umoren, S.A., Obot, I.B., 2008. Inhibition of Mild Steel Corrosion in Sulphuric Acid Using Alizarin Yellow GG Dye and Synergistic Iodide Additive. Int. J. Electrochem. Sci.3, 1325.
34. Chitra, S., Parameswari, K., Vidhya, M., Kalishwari, M., Selvaraj, A., 2011. Evaluation of Quinoxalines as Corrosion Inhibitors for Mild Steel in Acid Environment. Int. J. Electrochem.Sci., 6, 4593.
35. Obi-Egbedia, N.O., Essiena, K.E., Obotb, I.B., 2011.Computational simulation and corrosion inhibitive potential of alloxazine for mild steel in 1M HCl. J. Comput. Mol. Design., 1, 26.
36. Ahmed Yahya Issa Rubaye, Hassan Thamir Abdulsahib and Ali Abdulrazzaq Abdulwahid, Ali Abdulrazzaq Abdulwahid., 2015. Corrosion Inhibition Properties of Norepinephrine Molecules on Mild Steel in Acidic Media. J. Encapsulation. Adsor. Sci., 5, 155.
37. Mobin, M., Sheerin Masroo, 2012. Cationic Gemini Surfactants as Novel Corrosion Inhibitor for Mild Steel in 1M HCl. Int. J. Electrochem. Sci., 7, 6920.
38. Karthik, R., Muthukrishnan, P., Shen-Ming Chen, Jeyaprabha, B., Prakash, P., 2015. Anti-Corrosion Inhibition of Mild Steel in 1M Hydrochloric acid solution by using Tiliacora accuminata leaves Extract. Int. J. Electrochem. Sci.,10, 3707.
39. Hany, M., Abd El-Lateef., 2015. Experimental and computational investigation on the corrosion inhibition characteristics of mild steel by some novel synthesized imines in hydrochloric acid solutions. Corros. Sci., 92, 104.
40. Chakravarthy, M.P., Mohana, K.N., Pradeep Kumar, C.B., Badiea, A.M., 2015. Corrosion Inhibition Behaviour and Adsorption Characteristics of Dapsone Derivatives on Mild Steel in acid Medium. Ameri.Chem.Sci. 8 ,1.